Redox Biology 46 (2021) 102085

Contents lists available at ScienceDirect

Redox Biology

journal homepage: www.elsevier.com/locate/redox

Nox2-derived superoxide radical is crucial to control acute *Trypanosoma cruzi* infection

Carolina Prolo [a,b], Damián Estrada [a,b], Lucía Piacenza [a,b], Diego Benítez [c], Marcelo A. Comini [c], Rafael Radi [a,b,**], María Noel Álvarez [a,b,d,*]

[a] Departamento de Bioquímica, Facultad de Medicina, Universidad de la República, Montevideo, Uruguay
[b] Centro de Investigaciones Biomédicas (CEINBIO), Facultad de Medicina, Universidad de la República, Montevideo, Uruguay
[c] Laboratory Redox Biology of Trypanosomes, Institut Pasteur de Montevideo, Uruguay
[d] Departamento de Educación Médica, Facultad de Medicina, Universidad de la República, Montevideo, Uruguay

ARTICLE INFO

Keywords:
Superoxide radical
Trypanosoma cruzi
Macrophages
Nox2
Oxidative stress
Chagas disease

ABSTRACT

Trypanosoma cruzi is a flagellated protozoan that undergoes a complex life cycle between hematophagous insects and mammals. In humans, this parasite causes Chagas disease, which in thirty percent of those infected, would result in serious chronic pathologies and even death. Macrophages participate in the first stages of infection, mounting a cytotoxic response which promotes massive oxidative damage to the parasite. On the other hand, *T. cruzi* is equipped with a robust antioxidant system to repeal the oxidative attack from macrophages. This work was conceived to explicitly assess the role of mammalian cell-derived superoxide radical in a murine model of acute infection by *T. cruzi*. Macrophages derived from Nox2-deficient (gp91^{phox}-/-) mice produced marginal amounts of superoxide radical and were more susceptible to parasite infection than those derived from wild type (*wt*) animals. Also, the lack of superoxide radical led to an impairment of parasite differentiation inside gp91^{phox}-/- macrophages. Biochemical or genetic reconstitution of intraphagosomal superoxide radical formation in gp91^{phox}-/- macrophages reverted the lack of control of infection. Along the same line, gp91^{phox}-/- infected mice died shortly after infection. In spite of the higher lethality, parasitemia did not differ between gp91^{phox}-/- and *wt* animals, recapitulating an observation that has led to conflicting interpretations about the importance of the mammalian oxidative response against *T. cruzi*. Importantly, gp91^{phox}-/- mice presented higher and disseminated tissue parasitism, as evaluated by both qPCR- and bioimaging-based methodologies. Thus, this work supports that Nox2-derived superoxide radical plays a crucial role to control *T. cruzi* infection in the early phase of a murine model of Chagas disease.

1. Introduction

Trypanosoma cruzi (*T. cruzi*) is the protozoan microorganism causative of Chagas disease, endemic in Central and South America and now expanding to other world regions. It is estimated that seven million people are infected and another 28 million are at risk of infection [1]. *T. cruzi* is a highly adapted parasite, which can survive silently for years in host tissues. Upon transmission of infective parasites to the blood by a triatomine vector, circulating trypomastigotes penetrate tissues and invade mainly macrophages [2]; parasites are internalized to the macrophage phagosome where they can be eliminated or escape towards the cytosol and differentiate into the amastigote stage. Amastigotes proliferate and differentiate to trypomastigotes, which are then released extracellularly secondary to macrophage disruption. Then, trypomastigotes infect other cells and colonize numerous tissues, such as the heart and gastrointestinal tract [3,4].

While acute phase of infection is usually asymptomatic, 30% of patients can progress to a symptomatic chronic phase years later, which is characterized mainly by dilated cardiomyopathy and megaviscera, both pathologies being fatal. The determinant factors for the long-term

* Corresponding author. Departamento de Bioquímica, Facultad de Medicina, Universidad de la República, Avda. General Flores 2125, Montevideo, 11800, Uruguay.
** Corresponding author. Departamento de Bioquímica, Facultad de Medicina, Universidad de la República, Avda. General Flores 2125, Montevideo, 11800, Uruguay.
E-mail addresses: rradi@fmed.edu.uy (R. Radi), noelalv@fmed.edu.uy (M.N. Álvarez).

https://doi.org/10.1016/j.redox.2021.102085
Received 9 June 2021; Received in revised form 14 July 2021; Accepted 26 July 2021
Available online 31 July 2021

outcome of *T. cruzi* infection are still under investigation [5]. This and other questions remain unanswered and unraveling the molecular mechanisms underlying infection and host immune response is essential to improve therapies for patients. At this time there is no vaccine available for this disease and the approved chemotherapy is very limited and has important secondary effects [3].

T. cruzi is equipped with an extensive antioxidant network, and various enzymes of this system are considered virulence factors [6–8]. Such metabolic arrangement is in good part related to the redox nature of parasite interaction with host cells, as *T. cruzi* faces the oxidative attack of professional phagocytes as part of the first defense line of the innate immune response. In particular, two enzymatic mechanisms in mammalian macrophages turn phagosomes into an oxidative and hostile environment for invading microorganisms such as *T. cruzi*. First, phagocytosis and pathogen pattern recognition trigger the assembly of the NADPH oxidase 2 complex (Nox2), composed by two membrane-bound subunits (gp91 and p22) that form the flavocytochrome b_{558} and three cytosolic subunits (p47, p40 and p67). Nox2 assembly depends on the protein kinase-C (PKC) signaling pathway and small GTPase Rac activation, which promote the phosphorylation and migration of cytosolic subunits to the plasma membrane (and hence, phagosome membrane) to bind to flavocytochrome b_{558} and form the fully active complex [9,10]. The active site of Nox2 is oriented towards the lumen of the phagosome and catalyzes a burst of superoxide radical ($O_2^{\bullet-}$) production at the expense of oxygen and NADPH [11]. Inhibition or ablation of this enzyme has been shown to be detrimental for controlling the infection of a number of pathogens *in vitro* and *in vivo* [12–17]. In particular, early studies of macrophage cytotoxicity to *T. cruzi* already related the killing of the parasite to $O_2^{\bullet-}$ formation [18,19]. In spite of the moderate direct toxicity of $O_2^{\bullet-}$, secondary $O_2^{\bullet-}$-derived species have important deleterious effects on microorganisms [20]. At the phagosome lumen or upon entry to the parasite, $O_2^{\bullet-}$ can dismutate to hydrogen peroxide (H_2O_2) by the action of internalized extracellular superoxide dismutase (EC-SOD) [21,22] or *T. cruzi* Fe-SOD [20], respectively. H_2O_2 is a mild oxidant species capable of promoting oxidative modifications to biomolecules when present at high concentration [23]. Importantly, when macrophages are stimulated by pro-inflammatory stimulus (such as interferon-γ, produced by natural killer cells), they produce another free radical relevant for pathogen elimination: nitric oxide ($^{\bullet}$NO). Inducible nitric oxide synthase (iNOS or NOS2) is responsible for $^{\bullet}$NO synthesis in the context of the infection by a number of microorganisms and its cytotoxic effects are largely demonstrated [16,24–26]. Notably, when $^{\bullet}$NO and $O_2^{\bullet-}$ are simultaneously formed, they react inside the phagosome [13,27] to yield peroxynitrite ($ONOO^-$/ONOOH) [28], a strong oxidant and cytotoxic agent that becomes a key reactive intermediate for parasite killing [13,29]. While there has been a general agreement on the role of oxidants in controlling acute Chagas disease [13,18,19], recent works using gp91^{phox}-/- mice has challenged this view, suggesting that mammalian cell-derived oxidants may favor infection through pro-proliferative actions on *T. cruzi* [30,31]. This controversy for the redox field imposes further investigation.

In this work, the gp91^{phox}-/- mouse model is used to analyze *in vitro* and *in vivo* the role of oxidant production in the early stage of *T. cruzi* infection. These animals have a deletion in the gp91 gene, a modification responsible for chronic granulomatous disease (CGD) phenotype [15]. gp91 is the catalytic subunit of Nox2, the prototypical phagocytic isoform of NADPH oxidase, and hence macrophages and neutrophils of these mice, among other cell types, are unable to produce large amounts of $O_2^{\bullet-}$ or, as a consequence, H_2O_2 and peroxynitrite. The data presented here, provide further evidence on the key role of $O_2^{\bullet-}$ in the control of *T. cruzi in vitro* and *in vivo*.

2. Materials and methods

2.1. Reagents

Dulbecco's modified Eagle's medium (DMEM), Roswell Park Memorial Institute (RPMI), phorbol 12-myristate 13-acetate (PMA) were purchased from Sigma. Lab-Tek tissue culture chamber slides were from Nunc. Amplex Ultra Red, 4-6-Diamidino-2-phenylindole (DAPI), fetal bovine serum (FBS) and dihydroethidium (DHE) were from Invitrogen. Xanthine oxidase was purchased from Calbiochem and D-luciferin from Perkin Elmer. All other reagents were of research grade quality. gp91^{phox} mice were purchased from The Jackson Laboratory (#002365). C57BL/6 mice were obtained from Unidad de Animales Transgénicos y de Experimentación (UATE) of the Institut Pasteur de Montevideo. All animals were maintained under proper conditions according to local regulations and with the Comisión Nacional de Experimentación Animal (National Commission of Animal Experimentation) authorization.

2.2. Macrophage purification and differentiation

Primary cultures of murine bone marrow-derived macrophages were purified as described elsewhere [32]. Briefly, C57BL/6 and gp91^{phox}-/- mice were sacrificed and tibia and femur bones were dissected. Epiphyses were cut and bone marrow was flashed onto a centrifuge tube using a 25G needle loaded with RPMI medium. Bone marrow cells were washed twice with PBS, then counted and seeded at a density of 2×10^5 cells per well in eight-well chamber slides or 5 x 10^5 cells per well in 24-well plates. Cells were cultured for 7 days in RPMI supplemented with 10% heat-inactivated FBS and 30% v/v supernatant from the L929 cell line, which secrets macrophage colony-stimulating factor and promotes macrophage differentiation.

Peritoneal macrophages were obtained as described elsewhere [33]. Briefly, mice were euthanized and abdominal skin was removed to expose peritoneum. Then, 5 ml of ice-cold PBS was injected into the peritoneal cavity using a 10 ml syringe with 25G needle and gently massaged to promote cell detachment from peritoneum. Cell suspension was recovered from the peritoneal cavity with a syringe and washed twice with PBS. Then, cells were resuspended in RPMI and seeded as described above. Experiments were performed immediately after cell attachment to culture plates.

2.3. T. cruzi culture and differentiation

T. cruzi epimastigotes (DM28c and CL-Brener) were cultured at 28 °C in brain-heart infusion (BHI) medium as described previously [34]. Two different *T. cruzi* strains were used in order to rule out specific responses related to the parasite genotype. DM28c and CL-Brener belong to Tc.I and VI *Discrete typing units* (DTU) respectively, and are representative of genetically diverse natural occurring strains [35,36]. CL-Luc:Neon parasites, which express both luciferase and a variant of the yellow fluorescent protein (mNeonGreen), were kindly provided by Dr. Martin Taylor, with permissions of Dr. Bruce Branchini and Alelle Biotech, owners of the respective reporter genes contained in those cells [37]. These parasites were cultured in BHI containing hygromycin (150 μg/ml, Sigma). Epimastigotes were differentiated into the infective metacyclic stage under chemically defined conditions as described previously [38]. Metacyclic trypomastigotes were used to infect confluent Vero cells (American Type Culture Collection) at 37 °C in a 5% CO_2 atmosphere. Primary macrophages or mice were infected with culture-derived trypomastigotes obtained from Vero cells monolayers.

2.4. Macrophage infection with T. cruzi

Bone marrow or peritoneal macrophages were seeded in Lab-Tek tissue culture chamber incubated with cell culture-derived trypomastigotes (parasite:macrophage ratio of 5:1) for 2 h at 37 °C. Non-engulfed

parasites were removed by washing twice in PBS, and infected-macrophages were either fixed at this time point to evaluate invasion or further incubated for 24 h in DMEM at 37 °C. Infected macrophages were fixed in a 4% (v/v) formaldehyde solution in PBS for 10 min at room temperature, washed with PBS, and permeabilized for 5 min with 0.1% (v/v) Triton X-100 in PBS. The number of parasites per macrophage was determined by DAPI staining (5 μg/ml) and visualized through fluorescence microscopy at 1,000 × magnification (Nikon Eclipse TE-200 inverted microscope). At least 2,000 cells from 3 independent experiments were counted. Results are expressed as amastigotes per 100 macrophages. In another set of experiments infected macrophages were cultured for 5 additional days with daily replacement of culture medium. Trypomastigotes or amastigotes release was evaluated by collecting supernatant and centrifuging (3000 *g*, 5 min) to concentrate parasites and counting in a Neubauer chamber.

2.5. Biochemical reconstitution of intraphagosomal superoxide radical formation during infection

Xanthine oxidase was used as an enzymatic source of $O_2^{\bullet-}/H_2O_2$ [39] during *in vitro* infection in gp91^{phox}-/- macrophages. DM28c *T. cruzi* trypomastigotes (2 x 10^7) were pre-incubated with a solution of xanthine oxidase (150 mU/mL) during 20 min to promote protein attachment and then washed twice. gp91^{phox}-/- bone marrow macrophages were then infected with these xanthine oxidase-coated parasites and after 2 h of incubation, culture medium containing not-engulfed trypomastigotes was removed and xanthine (150 μM) was added as substrate for xanthine oxidase. Infection index was evaluated at 24 h post-infection.

The $O_2^{\bullet-}$ flux of xanthine oxidase-coated parasites was calculated as the difference of enzymatic activity in solution before and after trypomastigote incubation, as measured by the cytochrome *c* reduction assay (ε_{550}= 21 $mM^{-1}cm^{-1}$). It was estimated that the parasite suspension retained 50% of total enzymatic activity, *i.e.,* $O_2^{\bullet-}$ flux ~5.2 x 10^{-11} mol/min. Considering the number of trypomastigotes and assuming a homogenous distribution of the enzyme, it is possible to estimate a $O_2^{\bullet-}$ flux of 2.6 x 10^{-18} mol/min per trypomastigote.

2.6. Genetic gp91 protein reconstitution in gp91^{phox}-/- macrophages

Lentiviral particles containing the gp91 gene were generated using a 3rd generation system in 293T cells as established by the Broad Institute RNAi Consortium [40]. Plasmid carrying the gp91 gene (pLV.SP146. gp91.GP91.cHS4) was a gift from Didier Trono (Addgene plasmid #30480; http://n2t.net/addgene:30480; RRID:Addgene_30480) [41]. gp91^{phox}-/- bone marrow macrophages were transfected with lentiviral particles carrying the plasmid with the gp91 gene ("pLV.gp91") during differentiation. (2 days after extraction) with a ratio of 2:1 (lentiviral particles:cells). After full differentiation, cells were assayed for gp91 mRNA expression by PCR with specific primers (forward: 5'-ACTTCTTGGGTCAGCACTGG-3', reverse: 5'-GTTCCTGTCCAGTTG TCTTCG-3') as described in Ref. [42]. Respiratory burst was evaluated in transfected cells measuring H_2O_2-dependent Amplex Red oxidation in the presence of horseradish peroxidase (HRP, Sigma) and using PMA (4 μg/ml) as activator. Finally, killing capacity against *T. cruzi* was evaluated performing infection experiments as described above.

2.7. Superoxide radical detection

Wild type (*wt*) or gp91^{phox}-/- bone marrow macrophages (5 x 10^6) were incubated at 37°C for 40 min with dihydroethidium (DHE, 50 μM) and then cells were washed with PBS to eliminate non-incorporated probe. DHE-preloaded macrophages were activated with PMA (4 μg/ml) in Dulbecco's modified PBS (dPBS: NaCl, 137 mM; KCl, 2.7 mM; Na_2HPO4, 8 mM; KH_2PO_4, 1.45 mM; $CaCl_2$, 0.9 mM; $MgCl_2$, 0.5 mM; glucose, 5.5 mM; L-arginine, 1 mM). After 2 h of incubation, cells were harvested and lysed in PBS plus Triton X-100 (0.1% v/v) by passing 50 times through a syringe needle (27Gx1/2'' 0.4 × 13 mm). Organic extraction of DHE-derived products and protein precipitation were performed with acetonitrile (ACN, 100 μL, 120 min at 4 °C) [43]. Samples were centrifuged (16,000 g, 30 min at 4 °C), and organic phase was removed and dried in a vacuum evaporator at 40 °C, 100 mbar, and 40 rpm. Samples were resuspended in 100 μL of sample buffer [90% water; 10% ACN; and 0.1% trifluoroacetic acid (TFA)]. DHE-derived products [2-OH-E^+ and ethidium (E^+)] were separated by HPLC with a C_{18} column (250 × 4.6 mm, 2.7 μm) equilibrated with mobile phase (10% ACN, and 0.1% TFA in aqueous solution). Samples were eluted with a linear increase of ACN phase from 10 to 65% in 40 min (0.5 mL/min), and analytes monitored by fluorescence detection at 510 and 595 nm [44].

2.8. In vivo infection with T. cruzi

Female C57BL/6 and gp91^{phox}-/- mice (10 to 12 weeks old) were inoculated intraperitoneally (5 mice per group) with 1 × 10^7 culture-derived trypomastigotes. Animals were monitored daily for overall status. gp91^{phox}-/- mice do not survive infection further than 12 days after inoculation.

2.9. Parasitemia

From day 3 to 10 post inoculation with *T. cruzi* parasites, parasitemia was assayed on blood (3 μL) drawn from the tail tips of mice as described previously [45], and the number of trypomastigotes was counted in a Neubauer chamber at 400x magnification.

2.10. Tissue parasite burden

At day 10 post-infection, hearts and quadriceps (100 mg) from infected mice were recovered, washed, and homogenized in DNAzol (1 mL; Invitrogen) by using a glass homogenizer (5 to 10 strokes; Glas-Col). DNA was purified, and the amount of *T. cruzi* satellite DNA (195-bp fragment) was quantified by qPCR [46]. Total DNA (100 ng) was analyzed on a thermal cycler with Fast SYBR Green Master Mix (Applied Biosystems) with the specific primers 5'-AATTATGAATGGCGG-GAGTCA-3' (forward) and 5'-CCAGTGTGTGAACACGCAAAC-3' (reverse). The amount of mouse chromosomal DNA was quantified in parallel by qPCR using glyceraldehyde-3-phosphate dehydrogenase (GAPDH)-specific primers: 5'-CTGAGAACGGGAAGCTTGTC-3' (forward) and 5'-CCTGCTTCACCACCTTCTTG-3' (reverse). Each qPCR mixture (20 μL) included 2 × SYBR Green SuperMix (10 μL), 0.5 μM of each primer, and DNA (100 ng). The qPCR program consisted of one cycle at 50 °C (10 min) and 94 °C (3 min); 40 cycles of 94 °C (45 s), 68 °C (1 min), and 72 °C (1 min); and one cycle at 72 °C (10 min). The post amplification melting curve was analyzed by measuring the fluorescence between 95 and 55 °C. Fold change was calculated as $2^{-\Delta\Delta Ct}$, where ΔCt is the difference between the Ct value of *T. cruzi* and GAPDH; and ΔΔCt is the difference between the ΔCt of gp91^{phox}-/- and *wt* samples.

Spleen parasitism was evaluated by measuring fluorescence in organs obtained from *wt* and gp91^{phox}-/- mice infected with CL:LucNeon trypomastigotes. At 10 days post-infection (dpi), spleens were dissected and single-cell suspension was obtained by passing through a metallic mesh. Parasites-derived fluorescence was measured in a plate reader (Varioskan Flash, λ_{em} = 480, λ_{ex} =520). Total protein was quantitated by the bicinchoninic acid assay and fluorescence was normalized by protein concentration of the samples.

2.11. Bioimaging of T. cruzi-infected animals and tissues

gp91^{phox}-/- and C57BL/6 mice (n=5/groups) were infected intraperitoneally with CL-Luc:Neon trypomastigotes (1 x 10^7 per mouse) as described above. Importantly, the route of inoculation has been proved

to be unrelated to parasite distribution throughout the animal [47]. Bioluminescence was evaluated *in vivo* at day 3, 5, 7 and 10 post infection. For that purpose, animals were injected with D-luciferin (150 mg/kg) intraperitoneally, anesthetized with gaseous isoflurane (2.5 % v/v) in oxygen and placed in a multi-modal *in vivo* imaging system (In Vivo Xtreme II, Bruker). Bioluminiscence images were obtained (settings: High sensitivity mode, binning 4 x 4 pixels, 5 min exposure time, field of view 190 mm, fStop 5.6, focal plane 0, tray Focal reference), followed by a single X-ray scan (settings: high speed sensitivity mode, no binning, 4 s exposure time, field of view 190 mm, fStop 5.60, focal plane 0, X ray Focal reference). After imaging, animals were recovered and returned to cages. For *ex vivo* imaging at 11 dpi, mice were injected with 150 mg/kg with D-luciferin and after 7 min, exsanguinated under terminal anesthesia (pentobarbital, 100 mg/kg). Then, mice were intracardially perfused with 10 ml of D-luciferin (0.3 mg/ml) in PBS with a 25G needle. Organs and tissues were excised, transferred to a 15 mm Petri dish, soaked in D-luciferin (0.3 mg/ml) in pre-warmed PBS-glucose 1% w/v and then imaged at 37 °C in the luminescence modality as described above. Also, a reflectance image was obtained (high speed mode, no binning, 0.1 s exposure time, field of view 190 mm, fStop, 2.80 focal plane 0, tray Focal reference). Image analysis was performed in Fiji software (Image J). To quantitate total intensity of whole animal signal, "Integrated Density" parameter was measured for each mouse, considering an area of 95x270 pixels and then corrected for background (signal of an obscure area of the same size in the image). Relative change in signal intensity was calculated taking the first image (3 dpi) of each animal as reference.

2.12. Ethical statements

Mice were bred at the Institut Pasteur de Montevideo animal facilities under specific pathogen free (SPF) conditions and experiments were performed in Facultad de Medicina or in the aforementioned institute in compliance with Uruguayan laws (No. 18.611) and guidelines for the use of laboratory animals (protocols "Exp. N°070153-000119-15," "Exp.N°070153-000366-18") approved by the Facultad de Medicina, Universidad de la República ethics committee.

2.13. Statistical analysis

Data are expressed as mean ± SEM unless otherwise stated. Data were analyzed using the Student's *t*-test (comparison of two groups) or ANOVA (comparison of multiple groups). $p \leq 0.05$ was considered significant. All experiments were reproduced at least three times on independent days, with a minimum of two replicates.

3. Results

Nox2 deficiency leads to uncontrolled *T. cruzi* proliferation in macrophages. BMDM obtained from gp91^{phox}-/- mice were used to evaluate the relevance of Nox2 activity during *T. cruzi* infection. These macrophages lack the catalytic subunit of the Nox2 complex (gp91) and are unable to mount the classic oxidative burst observed in professional phagocytes [15]. For infection experiments, parasites and macrophages were co-incubated and non-internalized trypomastigotes were removed after 2 h. Macrophages and *T. cruzi* nuclei were stained and analyzed by epifluorescence microscopy (Fig. 1A) to determine the infection index (*T. cruzi*/100 macrophages, Fig. 1B–D) and the percentage of infected cells (Supp. Figure 1). Importantly, *T. cruzi* uptake was not affected by the genetic deficiency of gp91^{phox}-/- cells, given there was no difference in the number of internalized trypomastigotes in macrophages from gp91^{phox}-/- or *wt* mice (Fig. 1B.). However, results obtained after 24 h of infection, with both DM28c and CL-Brener *T. cruzi* strains, demonstrate that parasite proliferation is poorly controlled in naïve gp91^{phox}-/- bone marrow macrophages in relation to *wt* cells (Fig. 1C); a similar pattern was observed when peritoneal macrophages were infected with DM28c trypomastigotes (Fig. 1D).

After six days of infection, extracellular parasites were visible both in the *wt* and gp91^{phox}-/- macrophages cultures due to intracellular parasite proliferation and cell lysis (Fig. 2). Interestingly, while trypomastigotes were mainly found in the supernatant of *wt*-infected macrophages, amastigotes predominated in the supernatant of gp91^{phox}-/- infected macrophages (Fig. 2 and Supp. Figure 2).

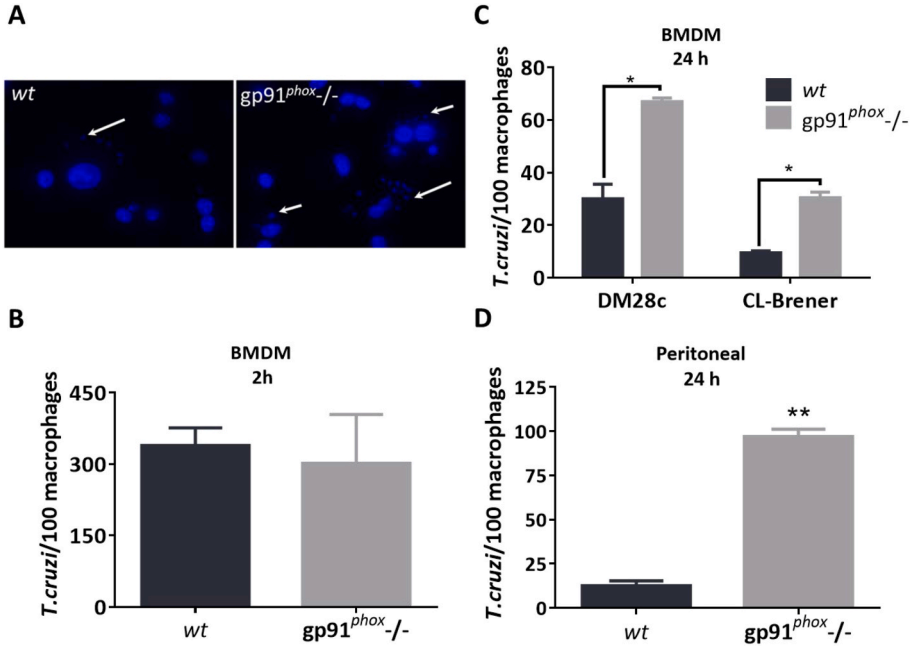

Fig. 1. gp91^{phox}-/- macrophages fail to control *T. cruzi* proliferation *in vitro*. *wt* and gp91^{phox}-/- primary macrophages were incubated with cell culture-derived trypomastigotes (parasite:macrophage ratio of 5:1) for 2 h at 37 °C. Non-engulfed parasites were removed and macrophages were further incubated for 24 h at 37 °C. Infected cultures were fixed and stained with DAPI for nuclei counting. The number of parasites every 100 macrophage was determined by fluorescence microscopy at 1,000X magnification. A) Representative images of DAPI-stained macrophage culture infected with DM28c strain (arrows pointing *T. cruzi* nuclei). B) BMDM infection index after 2h of incubation with DM28c parasites. C) BMDM infection index for CL-Brener and DM28 strains after 24 h. D) Peritoneal macrophages infection index with DM28c parasites.

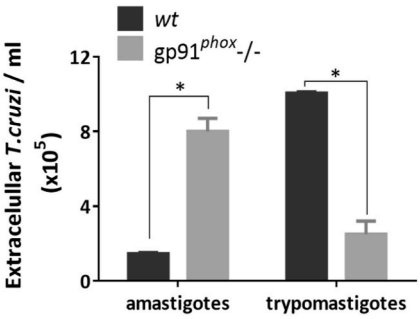

Fig. 2. Lack of intraphagosomal superoxide radical leads to amastigote release from gp91^{phox}-/- macrophages. *wt* and gp91^{phox}-/- bone marrow macrophages were incubated with cell culture-derived trypomastigotes (5:1) for 2 h at 37 °C. Non-engulfed parasites were removed and macrophages were further incubated for 6 days at 37 °C. Trypomastigotes and amastigotes recovered from the supernatant of infected macrophages were concentrated and counted in a Neubauer chamber at 400X magnification. "*" denotes $p<0.05$.

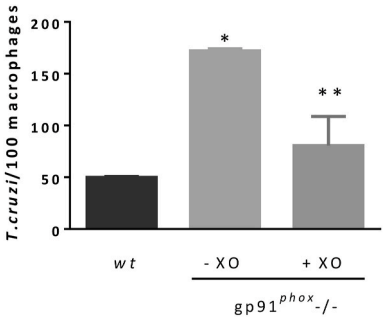

Fig. 4. Reconstitution of intraphagosomal superoxide radical formation during infection partially restores the cytotoxic capacity of gp91^{phox}-/- macrophages. gp91^{phox}-/- bone marrow macrophages were infected with cell culture-derived trypomastigotes (5:1, DM28c) previously coated with xanthine oxidase. After 2 h, non-engulfed parasites were removed, xanthine was added to culture medium (150 μM) and macrophages were further incubated for 24 h at 37 °C. Infection index was determined by counting DAPI-stained nuclei. RFU, relative fluorescence units. "**" denotes statistical differences respect to "*" with $p<0.05$. Nox2-KO mice are highly susceptible to *Trypanosoma cruzi* infection.

3.1. *Biochemical and genetic reconstitution of intraphagosomal superoxide radical formation partially restores the cytotoxic capacity of gp91^{phox}-/- macrophages*

In naïve *wt* macrophages the main reactive species formed during *T. cruzi* infection are $O_2^{\bullet-}$ and H_2O_2, the latter being formed through $O_2^{\bullet-}$ dismutation [13]. Nox2 is responsible for the massive production of these oxidants under classical stimulus in *wt* macrophages, while in the gp91^{phox}-/- macrophages, $O_2^{\bullet-}$ generation is largely decreased (Fig. 3). The $O_2^{\bullet-}$ flux measured in *wt* bone marrow macrophages through DHE oxidation was 2.8 pmol/min x 10^6 cells, while in gp91^{phox}-/- macrophages the rate of $O_2^{\bullet-}$ production was ~30 times less, *ca.* 0.1 pmol/min x 10^6 cells; the marginal flux of $O_2^{\bullet-}$ might come from other sources including mitochondria and other Nox isoforms.

To prove that the lack of $O_2^{\bullet-}$ explained the excessive intracellular proliferation of *T. cruzi* in gp91^{phox}-/- macrophages, infection experiments were performed with xanthine oxidase-coated trypomastigotes (see Materials and Methods). This experimental approach should provide an alternative source of relevant amounts of $O_2^{\bullet-}$ and H_2O_2 (xanthine oxidase/xanthine) to emulate Nox2 activity during first moments after phagocytosis. Infection was carried out as usual and after removing non-internalized parasites, xanthine was added as a cell permeable substrate for xanthine oxidase. In Fig. 4, results show that the cytotoxic potential of gp91^{phox}-/- macrophages against *T. cruzi* was partially restored (~60%) when $O_2^{\bullet-}$ and H_2O_2 formation was reconstituted by the action of parasite-bound xanthine oxidase as an alternative source of intraphagosomal oxidants.

Alternatively, partial restoration of Nox2 activity in KO macrophages by genetic complementation with a lentiviral vector encoding gp91^{phox} gene, proportionally restored their cytotoxic activity (Supp Figure 3). It is remarkable that irrespective of the limited success of the genetic complementation approach (gp91^{phox} levels: <10 % of *wt*), such modest increase of Nox2 activity consistently correlated with the extent of $O_2^{\bullet-}$ detection and cytotoxicity (*ca.* 10 % of *wt*).

Taken together, these results strengthen previous evidence regarding the relevance of Nox2 activity in controlling *T. cruzi* survival in macrophages [13,18,48].

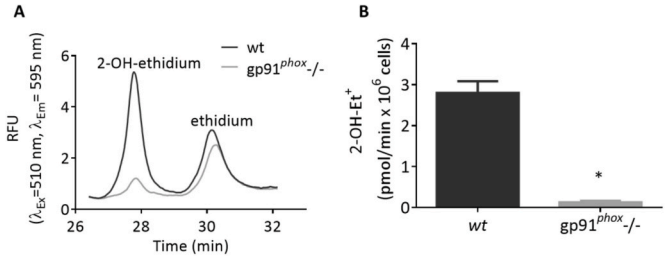

Fig. 3. Superoxide radical production in *wt* and gp91^{phox}-/- macrophages. A) *wt* or gp91^{phox}-/- bone marrow macrophages (2 x 10^6) were incubated for 40 min with DHE (50 μM) and then washed to eliminate non- incorporated probe. DHE-preloaded macrophages were treated with PMA (4 μg/ml) for 2 h. Then, DHE-derived products [2-OH-E^+ and ethidium (E^+)] were obtained by organic extraction, separated by HPLC and monitored by fluorescence detection (λ_{ex}=510 and λ_{em}=595 nm). A) Representative chromatogram is shown. B) Area under the curves was obtained from chromatograms for each type of macrophage and [2-OH-Et^+] was calculated by subtracting the signal obtained in non-activated cells and using a standard curve for 2-OH-E^+ (0–2 μM). "*" denotes $p<0.02$.

3.2. *Nox2-KO mice are highly susceptible to T. cruzi infection*

Next, the relevance of Nox2 in an acute Chagas disease model in mice was evaluated. Infection with DM28c strain of *T. cruzi* is lethal for gp91^{phox}-/- mice (Fig. 5A), as previously demonstrated for the same, and other strains [31,49,50]. In this experimental setting, all animals from the KO group died before the day 12 after inoculation. Despite the augmented lethality due to *T. cruzi* infection, the gp91^{phox}-/- mice showed a parasitemia similar to that of the control group (Fig. 5B). Nevertheless, tissue parasitism in typical organs invaded by *T. cruzi* evaluated by qPCR at 10 dpi, was significantly augmented in KO mice, *i. e.,* heart and skeletal muscle (Fig. 5C) evidencing the impaired ability to control parasite proliferation.

In order to have a broader perspective of *T. cruzi* invasion in gp91^{phox}-/- mice, the CL-Luc:Neon strain was used [37] for *in vivo* monitoring of infection by bioluminiscence. At different time points post-infection, animals were injected intraperitoneally with luciferase and red-shifted light emission recorded in an *in vivo* imaging system. Bioluminiscence reached a maximum intensity at day five for the *wt* group and decreased the following days (along with the decrease in parasitemia) while in the gp91^{phox}-/- mice, bioluminescence remained high until the end of experiment (Fig. 6A and B and Supp. Figure 4).

Ex vivo analysis of biodistribution of *T. cruzi* infection (11 dpi) is similar to that observed in previous reports [47] and showed that most of the tissues examined presented significantly higher bioluminescence signal in gp91^{phox}-/- than in *wt* animals (Fig. 6C). In particular, spleen, visceral fat and some sections of the gastrointestinal tract showed the most remarkable signal in KO mice.

Interestingly, vast spleen invasion has been involved in the lethality of *T. cruzi* infection with highly virulent strains. It is proposed that a

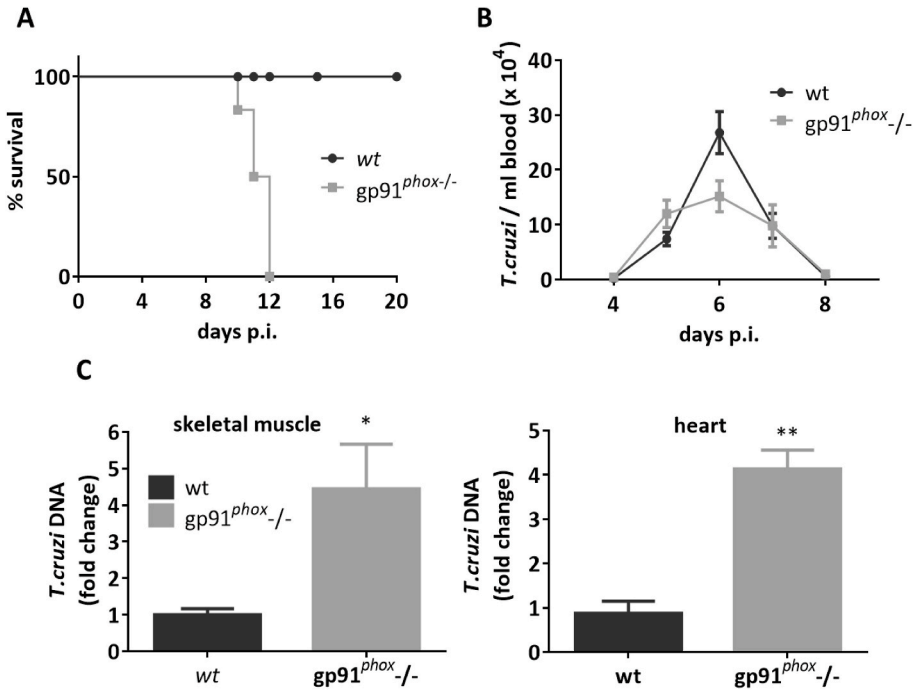

Fig. 5. Acute infection with *T. cruzi* in gp91^{phox}-/- mice. C57BL/6 and gp91^{phox}-/- mice (n=5 per group) were inoculated intraperitoneally with 1 × 10^7 culture-derived trypomastigotes and acute infection was evaluated by measuring (A) survival; (B) parasitemia and (C) tissue parasite burden by qPCR at 10 dpi. "*" denotes p=0.05 and "**" denotes p=0.02.

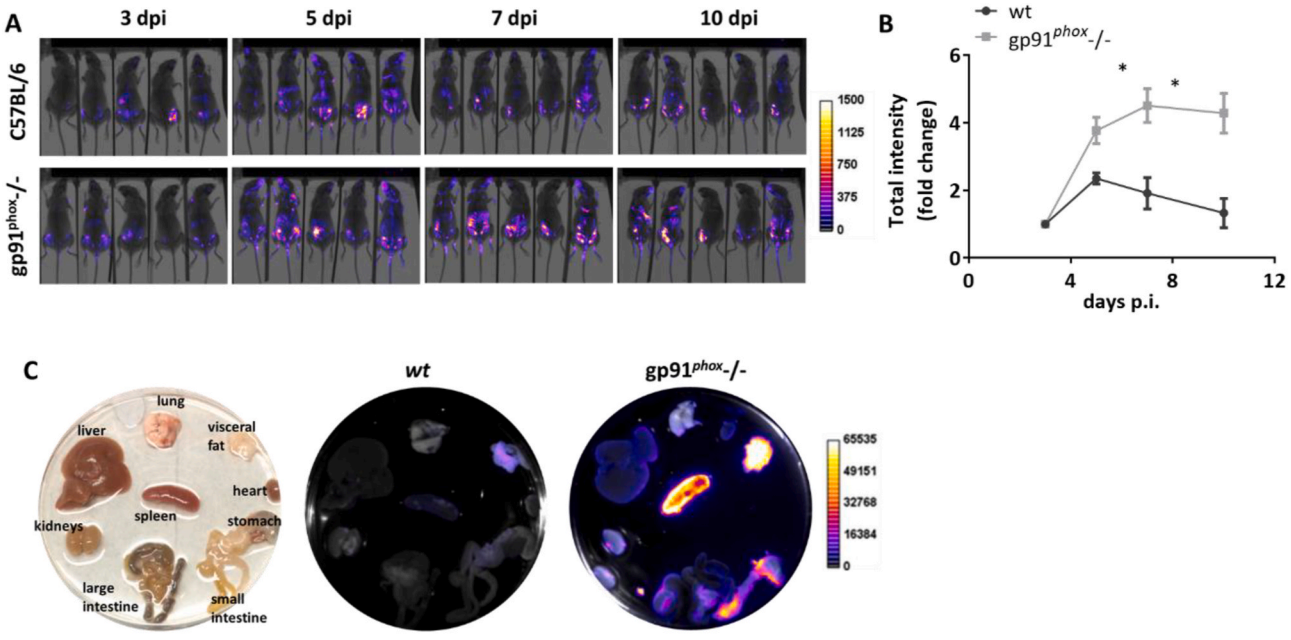

Fig. 6. *In vivo and ex vivo* imaging of *T. cruzi* infection in mice. gp91^{phox}-/- and C57Bl/6 mice (n = 5 per group) were infected with CL-Luc:Neon trypomastigotes (1 x 10^7 per mouse) intraperitoneally. A) On days 3, 5, 7 and 10 post infection, animals were injected intraperitoneally with D- luciferin 150 mg/kg and scanned by *in vivo* imaging system (In Vivo Xtreme II, Bruker). Superimposed images of bioluminescence and X-ray scan are shown. B) Results are expressed in terms of signal increment for each mouse from day 3 post infection (mean ± SEM). C) For *ex vivo* imaging at 11 dpi, representative animals from each group were injected with 150 mg/kg with D-luciferin intraperitoneally and perfused intracardially with 10 ml of D-luciferin (0.3 mg/ml). Organs and tissues were dissected, soaked in D-luciferin (0.3 mg/ml) in PBS-1% glucose w/v, and imaged. "*" denotes statistical difference with p=0.05.

massive destruction of splenic infected macrophages and the concomitant release of pro-inflammatory factors could lead to the collapse of the animal [51,52]. *T. cruzi* parasitism in spleen was analyzed taking advantage of the fluorescent parasites CL-Luc:Neon. Total fluorescence intensity was measured in single cell suspensions obtained from spleens of infected mice and it was confirmed that there is a pronounced parasite invasion in the spleens of gp91^{phox}-/- compared to *wt* mice (*ca.* seven times higher) (Fig. 7).

Thus, it was demonstrated that Nox2 deficiency led to a global and uncontrolled proliferation of *T. cruzi* in different host's tissues and

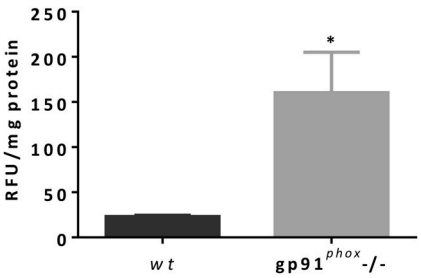

Fig. 7. Spleen parasitism in *T. cruzi*-infected mice. gp91^{phox}-/- and C57Bl/6 mice were infected with CL-Luc:Neon trypomastigotes (1 x 10^7 per mouse) intraperitoneally. At ten dpi, animals were euthanized and spleens were dissected. Single cell suspensions, obtained through mechanical disruption of spleen tissue, were analyzed in a plate fluorimeter to detect mNeon-derived fluorescence of *T.cruzi* parasites (λ_{ex}=480 and λ_{em}=520 nm). Data was normalized by total protein in lysates. "*" denotes $p < 0.05$.

organs.

4. Discussion

Reactive oxygen and nitrogen species are produced in the context of innate immune response by macrophages and neutrophils through specialized enzymes such as Nox2 and iNOS. In particular, *T. cruzi* infection constitutes a prototypical model of host-parasite interaction, where host-derived oxidants and the parasite antioxidant network interplay is crucial to the outcome of infection. It is well established that mice lacking interferon gamma (IFNγ-/-), are unable to control infection, due to impaired inflammatory signaling and iNOS expression [53]. Also, inhibition or genetic ablation of iNOS results in poor control of parasite proliferation, which in conjunction with *in vitro* toxicity experiments underscore the importance of $^{\bullet}$NO formation during *T. cruzi* infection [25,54]. On the other hand, the modulation of the parasite antioxidant enzyme content has reinforced the key role played by $O_2^{\bullet-}$ and its secondary oxidizing intermediates (*i.e.* H_2O_2 and $ONOO^-$) in host defense [6]. For instance, macrophage infection with *T. cruzi* strains overexpressing cytosolic Fe-SOD results in uncontrolled parasite proliferation due to augmented parasite $O_2^{\bullet-}$ detoxification [20]. Moreover, *T. cruzi* strains overexpressing peroxiredoxins, thiol-containing peroxidases capable of efficiently detoxifying intraphagosomal $ONOO^-$ and H_2O_2, are significantly more virulent than their *wt* counterparts *in vitro* and *in vivo* [13,55].

In this work, a gp91^{phox}-/- mouse model was used to explore the role of $O_2^{\bullet-}$ in controlling *T. cruzi* proliferation *in vitro* and *in vivo*. Genetic deficiency of Nox2 in mammalian cells leads to marginal $O_2^{\bullet-}$ formation during macrophage activation (~30 times less respect to that of *wt*). Concomitantly, bone marrow or peritoneal macrophages derived from gp91^{phox}-/- mice have a remarkable susceptibility to *T. cruzi* infection, which is not explained by differences in parasite internalization (Fig. 1B) but rather, by an impairment on the inhibition of proliferation or elimination by the host cell. This phenomenon is overcome when an exogenous source of $O_2^{\bullet-}$ is provided to the phagosome from the very early stage of pathogen internalization. Prior works with a $O_2^{\bullet-}$ production defective macrophage cell line variant showed that reconstitution of intraphagosomal oxidant ThO_2 formation with an alternative enzymatic source of H_2O_2 (*i.e.* zymosan particles covalently coupled with glucose oxidase), during *T. cruzi* phagocytosis restored cytotoxic activity [19,48]. Here, xanthine oxidase-coated *T. cruzi* was used as a $O_2^{\bullet-}$ generating system that upon phagocytosis generated an estimated flux of 2,6 x 10^{-18} mol/min per phagosome. When this flux is confined in a narrow volume as it is the phagosome (~ 3 fL, [20]), the maximum estimated rate is 0.87 mM/min. Such $O_2^{\bullet-}$ flux is comparable to that calculated for *wt* bone marrow macrophages if the measured rate of $O_2^{\bullet-}$ formation (Fig. 3) is extrapolated to intraphagosomal formation (0.9 mM/min, considering one phagosome per macrophage). It is important to bear in mind that the measured $O_2^{\bullet-}$ flux in *wt* BMDM through DHE oxidation represents a lower estimate, due to a number of limitations of the technique [56] Also, xanthine oxidase generates both $O_2^{\bullet-}$and H_2O_2, and under the experimental conditions of these assays the estimated "univalent flux" (the percentage of oxygen consumption related to $O_2^{\bullet-}$ formation) is ~30% [57,58]. Thus, according to these estimations, it is consistent to see a 60% recovery of cytotoxic capacity *via* xanthine oxidase in gp91^{phox}-/- macrophages. In the same line, partial genetic reconstitution of gp91 protein through lentiviral-mediated expression, led to moderate recovery of the cytotoxicity in gp91^{phox}-/- infected macrophages.

Importantly, genetic deficiency of phagocytic Nox2 results to be lethal for mice infected with *T. cruzi* (Fig. 5, A), which is in line with previous reports in literature. However, works from different labs, including ours, have not found any differences in the amount of parasites circulating in the blood of *wt vs* gp91^{phox}-/- infected mice [31,49,50], leading to the misconception that $O_2^{\bullet-}$ is not relevant in controlling *T. cruzi* proliferation *in vivo* [30,31,49]. Also, one work studied the tissue parasitism in the heart, spleen and liver from *T. cruzi*-infected mice, not being able to observe statistically significant differences in the amount of parasite-DNA among *wt* and gp91^{phox}-/- mice [49]. Nevertheless, in this work we found a remarkable higher parasite load in tissues of infected animals, indicative of gp91^{phox}-/- impaired capacity to control parasite proliferation in accordance with reports for other Nox2-deficiency models [17,59].

It might seem contradictory that, in spite of the high lethality observed in gp91^{phox}-/- mice, the level of organ and tissue compromise does not correlate with parasitemia since blood trypomastigotes stem from infected and lysed cells form tissues. Nevertheless, highly susceptible gp91^{phox}-/- macrophages released mainly amastigotes (Fig. 2), which could have implications regarding parasite dissemination in vicinal tissues of the Nox2-defective mice. Amastigotes could infect locally [60,61], augmenting tissue invasion without contributing to blood parasitemia. This could be explained at least by two factors: impaired differentiation from amastigote to trypomastigote in the absence of respiratory burst or premature cell lysis before full differentiation is accomplished, due to massive parasite proliferation inside cells. In either case, this observation helps to explain why blood parasitemia is not augmented in the highly susceptible gp91^{phox}-/-. Also, the role of the spleen in capturing circulatory parasites [62] and the important invasion observed in gp91^{phox}-/- spleens respect to that of *wt* animals could contribute to explain the unexpectedly low parasitemia.

Some works attribute a detrimental role in host defense to macrophage-derived oxidants in the context of *T. cruzi* infection, proposing that the parasite benefits from other possible effects of $O_2^{\bullet-}$ and its derivatives [30,31]. Although it has been described that low levels of H_2O_2 have a pro-proliferative role in the replicative epimastigotes and in the process of amastigogenesis [63–65] and also, an increment of the antioxidant enzymes content is observed in trypomastigotes upon incubation with low doses of H_2O_2 [66], the amounts of H_2O_2, $O_2^{\bullet-}$ and $ONOO^-$ (micromolar to millimolar range, [20,67,68]) faced by the parasite inside the phagosome are highly cytotoxic and opposed to a pro-proliferative role. It is important to bear in mind that differences in the content of antioxidant enzymes among *T.cruzi* strains may account for the variability in the susceptibility to the oxidative attack of phagocytic cells [69–71]. For example, macrophage infection with parasites overexpressing Fe-SOD-B, which are capable of detoxifying intra-parasite superoxide, leads to similar infection index in *wt* and gp91^{phox}-/- macrophages [20].

It was previously reported that Nox2 deficiency in p47^{phox}-/- mice leads to poor $CD8^+$ T cell activation, limiting the effectiveness of the immune response against *T. cruzi* [17]. Also, surplus $^{\bullet}$NO in the absence of a key modulator of its half -life, such as $O_2^{\bullet-}$, could aggravate pathology in gp91^{phox}-/- mice due to excessive $^{\bullet}$NO-mediated vasodilation, although this isolated factor does not account for mice mortality since

blood pressure restoration did not improve survival [49]. Incremented levels of •NO in gp91^{phox}-/- can also promote a pro-arrhythmogenic phenotype in cardiomyocytes, contributing to cardiac pathology in those animals [50].

Although it is reasonable to hypothesize that various mechanisms may contribute to lethality in *T. cruzi*-infected gp91^{phox}-/- mice, this work provides conclusive support for a crucial role of $O_2^{\bullet-}$ in the control of parasite tissue dissemination; in particular, Nox2 activity in macrophages results in intraphagosomal formation of $O_2^{\bullet-}$ and $O_2^{\bullet-}$ -derived reactive species which are required to neutralize parasite proliferation and disrupt its differentiation in the early stages of acute *T. cruzi* infection.

Declaration of competing interest

The authors declare that they have no known competing financial interests or personal relationships that could have appeared to influence the work reported in this paper.

Acknowledgments

We thank Lic. Mariela Santos and Dr. Martín Breijo for assistance in the use of animals and Dr. Celia Quijano for providing the plasmids for lentiviral particles production. Dr. Martin Taylor kindly provided the CL-Luc:Neon *T. cruzi* strain. Dr. Bruce Branchini and Allele Biotech developed the luciferase gene (PpyRE9h) and mNeonGreen protein expressed in those parasites. C.P. and D.E. were funded by fellowships of the Comisión Académica de Posgrado, Universidad de la República and Agencia Nacional de Investigación e Innovación, respectively.

This work was supported by grants from Universidad de la República: Espacio Interdisciplinario (to R.R.), Comisión Sectorial de Investigación Científica Grants Ini-2013-346 (to C.P.), I+D-2016 (to L.P., C. P., and M.N.A.), and Grupos 2018 (to R.R.). Additional support was obtained from Programa de Desarrollo de Ciencias Básicas (PEDECIBA, Uruguay). D.B. and M.A.C. thank the support of FOCEM (Fondo para la Convergencia Estructural del Mercosur, COF 03/11). All authors belong to the Sistema Nacional de Investigadores (SNI, Uruguay).

Appendix A. Supplementary data

Supplementary data to this article can be found online at https://doi.org/10.1016/j.redox.2021.102085.

References

[1] WHO, Chagas disease, . 11/03/2020 [cited 2021 22/01], https://www.who.int/news-room/fact-sheets/detail/chagas-disease-(american-trypanosomiasis). (Accessed January 2021).
[2] F. Kierszenbaum, et al., Phagocytosis: a defense mechanism against infection with Trypanosoma cruzi, J. Immunol. 112 (5) (1974) 1839–1844.
[3] A.F. Francisco, et al., Challenges in Chagas disease drug development, Molecules 25 (12) (2020).
[4] F. Köberle, Chagas' disease and Chagas' syndromes: the pathology of American trypanosomiasis, Adv. Parasitol. 6 (1968) 63–116.
[5] F. Cardillo, et al., Immunity and immune modulation in Trypanosoma cruzi infection, Pathog Dis 73 (9) (2015) ftv082.
[6] L. Piacenza, M. Trujillo, R. Radi, Reactive species and pathogen antioxidant networks during phagocytosis, J. Exp. Med. 216 (3) (2019) 501–516.
[7] L. Piacenza, et al., Enzymes of the antioxidant network as novel determiners of Trypanosoma cruzi virulence, Int. J. Parasitol. 39 (13) (2009) 1455–1464.
[8] F. Irigoin, et al., Insights into the redox biology of Trypanosoma cruzi: trypanothione metabolism and oxidant detoxification, Free Radic. Biol. Med. 45 (6) (2008) 733–742.
[9] B.M. Babior, The respiratory burst of phagocytes, J. Clin. Invest. 73 (3) (1984) 599–601.
[10] Y. Groemping, K. Rittinger, Activation and assembly of the NADPH oxidase: a structural perspective, Biochem. J. 386 (Pt 3) (2005) 401–416.
[11] G.L. Babior, et al., Arrangement of the respiratory burst oxidase in the plasma membrane of the neutrophil, J. Clin. Invest. 67 (6) (1981) 1724–1728.
[12] M.B.H. Carneiro, et al., N_{OX}2-Derived reactive oxygen species control inflammation during leishmania amazonensis infection by mediating infection-induced neutrophil apoptosis, J. Immunol. 200 (1) (2018) 196–208.
[13] M.N. Alvarez, et al., Intraphagosomal peroxynitrite as a macrophage-derived cytotoxin against internalized Trypanosoma cruzi: consequences for oxidative killing and role of microbial peroxiredoxins in infectivity, J. Biol. Chem. 286 (8) (2011) 6627–6640.
[14] L. Yi, et al., p47(phox) directs murine macrophage cell fate decisions, Am. J. Pathol. 180 (3) (2012) 1049–1058.
[15] J.D. Pollock, et al., Mouse model of X-linked chronic granulomatous disease, an inherited defect in phagocyte superoxide production, Nat. Genet. 9 (2) (1995) 202–209.
[16] M.U. Shiloh, et al., Phenotype of mice and macrophages deficient in both phagocyte oxidase and inducible nitric oxide synthase, Immunity 10 (1) (1999) 29–38.
[17] M. Dhiman, N.J. Garg, P47phox-/- mice are compromised in expansion and activation of CD8+ T cells and susceptible to Trypanosoma cruzi infection, PLoS Pathog. 10 (12) (2014), e1004516.
[18] C. Nathan, et al., Activation of macrophages in vivo and in vitro. Correlation between hydrogen peroxide release and killing of Trypanosoma cruzi, J. Exp. Med. 149 (5) (1979) 1056–1068.
[19] Y. Tanaka, et al., Reconstitution of a variant macrophage cell line defective in oxygen metabolism with a H2O2-generating system, Proc Natl Acad Sci U S A 79 (8) (1982) 2584–2588.
[20] A. Martinez, et al., Cytosolic Fe-superoxide dismutase safeguards Trypanosoma cruzi from macrophage-derived superoxide radical, Proc Natl Acad Sci U S A 116 (18) (2019) 8879–8888.
[21] M.L. Manni, et al., Extracellular superoxide dismutase in macrophages augments bacterial killing by promoting phagocytosis, Am. J. Pathol. 178 (6) (2011) 2752–2759.
[22] L. Hu, et al., The dynamic uptake and release of SOD3 from intracellular stores in macrophages modulates the inflammatory response, Redox Biol 26 (2019) 101268.
[23] C.C. Winterbourn, Biological chemistry of superoxide radicals, ChemTexts 6 (1) (2020) 7.
[24] C. Bogdan, Nitric oxide synthase in innate and adaptive immunity: an update, Trends Immunol. 36 (3) (2015) 161–178.
[25] C. Holscher, et al., Defective nitric oxide effector functions lead to extreme susceptibility of Trypanosoma cruzi-infected mice deficient in gamma interferon receptor or inducible nitric oxide synthase, Infect. Immun. 66 (3) (1998) 1208–1215.
[26] V.E. Laubach, et al., Mice lacking inducible nitric oxide synthase are not resistant to lipopolysaccharide-induced death, Proc Natl Acad Sci U S A 92 (23) (1995) 10688–10692.
[27] C. Prolo, et al., Nitric oxide diffusion to red blood cells limits extracellular, but not intraphagosomal, peroxynitrite formation by macrophages, Free Radic. Biol. Med. 87 (2015) 346–355.
[28] R. Kissner, et al., Formation and properties of peroxynitrite as studied by laser flash photolysis, high-pressure stopped-flow technique, and pulse radiolysis, Chem. Res. Toxicol. 10 (11) (1997) 1285–1292.
[29] M.N. Alvarez, et al., Macrophage-derived peroxynitrite diffusion and toxicity to Trypanosoma cruzi, Arch. Biochem. Biophys. 432 (2) (2004) 222–232.
[30] C.N. Paiva, et al., Oxidative stress fuels Trypanosoma cruzi infection in mice, J. Clin. Invest. 122 (7) (2012) 2531–2542.
[31] G.R. Goes, et al., Trypanosoma cruzi needs a signal provided by reactive oxygen species to infect macrophages, PLoS Neglected Trop. Dis. 10 (4) (2016), e0004555.
[32] K.D. Choi, M. Vodyanik, I.I. Slukvin, Hematopoietic differentiation and production of mature myeloid cells from human pluripotent stem cells, Nat. Protoc. 6 (3) (2011) 296–313.
[33] X. Zhang, R. Goncalves, D.M. Mosser, The isolation and characterization of murine macrophages, Curr. Protoc. Im. Supplement 83 (2008). Unit 14 1.
[34] L. Piacenza, G. Peluffo, R. Radi, L-arginine-dependent suppression of apoptosis in Trypanosoma cruzi: contribution of the nitric oxide and polyamine pathways, Proc Natl Acad Sci U S A 98 (13) (2001) 7301–7306.
[35] N.R. Sturm, et al., Evidence for multiple hybrid groups in Trypanosoma cruzi, Int. J. Parasitol. 33 (3) (2003) 269–279.
[36] B. Zingales, et al., The revised Trypanosoma cruzi subspecific nomenclature: rationale, epidemiological relevance and research applications, Infect. Genet. Evol. 12 (2) (2012) 240–253.
[37] F.C. Costa, et al., Expanding the toolbox for Trypanosoma cruzi: a parasite line incorporating a bioluminescence-fluorescence dual reporter and streamlined CRISPR/Cas9 functionality for rapid in vivo localisation and phenotyping, PLoS Neglected Trop. Dis. 12 (4) (2018) e0006388.
[38] V.T. Contreras, et al., In vitro differentiation of Trypanosoma cruzi under chemically defined conditions, Mol. Biochem. Parasitol. 16 (3) (1985) 315–327.
[39] L. Castro, M.N. Alvarez, R. Radi, Modulatory role of nitric oxide on superoxide-dependent luminol chemiluminescence, Arch. Biochem. Biophys. 333 (1) (1996) 179–188.
[40] Broad Institute. Genetic Perturbation Platform Portal.
[41] I. Barde, et al., Lineage- and stage-restricted lentiviral vectors for the gene therapy of chronic granulomatous disease, Gene Ther. 18 (11) (2011) 1087–1097.
[42] S.H. Lee, et al., Calcium-independent phospholipase A2beta-Akt signaling is involved in lipopolysaccharide-induced NADPH oxidase 1 expression and foam cell formation, J. Immunol. 183 (11) (2009) 7497–7504.
[43] D. Estrada, et al., Cardiomyocyte diffusible redox mediators control Trypanosoma cruzi infection: role of parasite mitochondrial iron superoxide dismutase, Biochem. J. 475 (7) (2018) 1235–1251.
[44] J. Zielonka, et al., Mechanistic similarities between oxidation of hydroethidine by Fremy's salt and superoxide: stopped-flow optical and EPR studies, Free Radic. Biol. Med. 39 (7) (2005) 853–863.

[45] T.C.d.C. Araújo-Jorge, Solange Lisboa de, *Doença de chagas: manual para experimentação animal*, vol. 368, Editora FIOCRUZ, 2000.
[46] S. Khare, et al., Proteasome inhibition for treatment of leishmaniasis, Chagas disease and sleeping sickness, Nature 537 (7619) (2016) 229–233.
[47] M.D. Lewis, et al., Bioluminescence imaging of chronic Trypanosoma cruzi infections reveals tissue-specific parasite dynamics and heart disease in the absence of locally persistent infection, Cell Microbiol. 16 (9) (2014) 1285–1300.
[48] Y. Tanaka, H. Tanowitz, B.R. Bloom, Growth of Trypanosoma cruzi in a cloned macrophage cell line and in a variant defective in oxygen metabolism, Infect. Immun. 41 (3) (1983) 1322–1331.
[49] H.C. Santiago, et al., NADPH phagocyte oxidase knockout mice control Trypanosoma cruzi proliferation, but develop circulatory collapse and succumb to infection, PLoS Neglected Trop. Dis. 6 (2) (2012), e1492.
[50] A. Santos-Miranda, et al., Reactive oxygen species and nitric oxide imbalances lead to in vivo and in vitro arrhythmogenic phenotype in acute phase of experimental Chagas disease, PLoS Pathog. 16 (3) (2020), e1008379.
[51] Z. Cordeiro. Kinetics of Trypanosoma Cruzi Destruction IN the Mouse Spleen, Revista da Sociedade Brasileira de Medicina Tropical, 1997, p. 30.
[52] E.S. Lima, Z.A. Andrade, S.G. Andrade, TNF-alpha is expressed at sites of parasite and tissue destruction in the spleen of mice acutely infected with Trypanosoma cruzi, Int. J. Exp. Pathol. 82 (6) (2001) 327–336.
[53] G.A. Martins, et al., Gamma interferon modulates CD95 (Fas) and CD95 ligand (Fas-L) expression and nitric oxide-induced apoptosis during the acute phase of Trypanosoma cruzi infection: a possible role in immune response control, Infect. Immun. 67 (8) (1999) 3864–3871.
[54] G.N. Vespa, F.Q. Cunha, J.S. Silva, Nitric oxide is involved in control of Trypanosoma cruzi-induced parasitemia and directly kills the parasite in vitro, Infect. Immun. 62 (11) (1994) 5177–5182.
[55] M.D. Pineyro, et al., Peroxiredoxins from Trypanosoma cruzi: virulence factors and drug targets for treatment of Chagas disease? Gene 408 (1–2) (2008) 45–50.
[56] J. Zielonka, M. Hardy, B. Kalyanaraman, HPLC study of oxidation products of hydroethidine in chemical and biological systems: ramifications in superoxide measurements, Free Radic. Biol. Med. 46 (3) (2009) 329–338.
[57] R. Radi, et al., Xanthine oxidase binding to glycosaminoglycans: kinetics and superoxide dismutase interactions of immobilized xanthine oxidase-heparin complexes, Arch. Biochem. Biophys. 339 (1) (1997) 125–135.
[58] I. Fridovich, Quantitative aspects of the production of superoxide anion radical by milk xanthine oxidase, J. Biol. Chem. 245 (16) (1970) 4053–4057.
[59] M. Dhiman, N.J. Garg, NADPH oxidase inhibition ameliorates Trypanosoma cruzi-induced myocarditis during Chagas disease, J. Pathol. 225 (4) (2011) 583–596.
[60] V. Ley, et al., Amastigotes of Trypanosoma cruzi sustain an infective cycle in mammalian cells, J. Exp. Med. 168 (2) (1988) 649–659.
[61] E.R. Ferreira, et al., Trypanosoma cruzi extracellular amastigotes and host cell signaling: more pieces to the puzzle, Front. Immunol. 3 (2012) 363.
[62] M. van Lookeren Campagne, A. Verschoor, Pathogen clearance and immune adherence "revisited": immuno-regulatory roles for CRIg, Semin. Immunol. 37 (2018) 4–11.
[63] J.K. Finzi, et al., Trypanosoma cruzi response to the oxidative stress generated by hydrogen peroxide, Mol. Biochem. Parasitol. 133 (1) (2004) 37–43.
[64] N.P. Nogueira, et al., Proliferation and differentiation of Trypanosoma cruzi inside its vector have a new trigger: redox status, PloS One 10 (2) (2015), e0116712.
[65] J.I.O. Paula, et al., New perspectives for hydrogen peroxide in the amastigogenesis of Trypanosoma cruzi in vitro, Biochim. Biophys. Acta (BBA) - Mol. Basis Dis. 1866 (12) (2020) 165951.
[66] F.R. Gadelha, et al., Release of the cytosolic tryparedoxin peroxidase into the incubation medium and a different profile of cytosolic and mitochondrial peroxiredoxin expression in H2O2-treated Trypanosoma cruzi tissue culture-derived trypomastigotes, Exp. Parasitol. 133 (3) (2013) 287–293.
[67] N. Rios, et al., Sensitive detection and estimation of cell-derived peroxynitrite fluxes using fluorescein-boronate, Free Radic. Biol. Med. (2016).
[68] C.C. Winterbourn, A.J. Kettle, Redox reactions and microbial killing in the neutrophil phagosome, Antioxidants Redox Signal. 18 (6) (2013) 642–660.
[69] A.A. Mielniczki-Pereira, et al., Trypanosoma cruzi strains, Tulahuen 2 and Y, besides the difference in resistance to oxidative stress, display differential glucose-6-phosphate and 6-phosphogluconate dehydrogenases activities, Acta Trop. 101 (1) (2007) 54–60.
[70] M.P. Zago, et al., TcI isolates of trypanosoma cruzi exploit the antioxidant network for enhanced intracellular survival in macrophages and virulence in mice, Infect. Immun. 84 (6) (2016) 1842–1856.
[71] L. Piacenza, et al., Trypanosoma cruzi antioxidant enzymes as virulence factors in Chagas disease, Antioxidants Redox Signal. 19 (7) (2013) 723–734.